Exp Fluids
DOI 10.1007/s00348-006-0184-z

RESEARCH ARTICLE

A colorimetric reaction to quantify fluid mixing

Peter M. Oates · Charles F. Harvey

Received: 22 October 2005 / Revised: 4 May 2006 / Accepted: 1 June 2006

Abstract We found the colorimetric reaction of Tiron (1,2-dihydroxybenzene-3,5-disulfonic acid) and molybdate suitable for optical quantification of chemical reaction during fluid–fluid mixing in laboratory chambers. This reaction consists of two colorless reagents that mix to rapidly form colored, stable, soluble products. These products can be digitally imaged and quantified using light absorbance to study fluid–fluid mixing. Here we provide a model and equilibrium constants for the relevant complexation reactions. We also provide methods for relating light absorbance to product concentrations. Practical implementation issues of this reaction are discussed and an example of imaged absorbances for fluid–fluid mixing in heterogeneous porous media is given.

1 Introduction

Understanding chemical reaction during fluid–fluid mixing is important for environmental processes (Beven et al. 1994), the chemical industry (Sterbacek and Tausk 1965), pharmaceutical engineering (Hickey and Ganderton 2001), process industries (Harnby et al. 1985), and the field of medicine (Omurtag et al. 1996; International Union of Biochemistry 1964) among other disciplines. Reactive mixing results from molecular diffusion across complex fluid–fluid interfaces (Ottino 1990).

To better understand this molecular-scale phenomenon, researchers have developed noninvasive optical measurement techniques. The two leading methods are laser-induced fluorescence, where the fluorescence of a reaction product is measured (e.g. Koochesfahani and Dimotakis 1985), and absorption imaging, where the amount of light absorbance is related to chemical concentration by Beer's Law (Tidwell and Glass 1994; Zhang et al. 1995; Gramling et al. 2002). As pointed out by Zhang et al. (1995), planar-laser-induced fluorescence (PLIF) is an excellent technique but involves a relatively complex setup; requiring laser equipment and special mirrors to separate the laser into a plane. This light plane is able to able to give a 2D concentration profile at a selected location in the mixing vessel. However, experimental times are typically short to avoid changes in the fluorescent signal due to temperature variation (e.g. Kling and Mewes 2003). Absorption imaging involves a simpler setup by pairing a colorimetric chemical reaction with a charge-coupled device (CCD) camera and digital image processing to quantify the 2D absorption field (Tidwell and Glass 1994; Zhang et al. 1995; Gramling et al. 2002). Experimental times can typically be much longer implying this technique maybe more suitable for studying slower flows (Zinn et al. 2004). Absorption imaging is a quasi-2D technique that is unable to resolve concentration detail in the third spatial dimension but it does provide the correct spatial average of the molecular product formed. Whether the correct spatial average of product formation given by absorption imaging or a plane giving detailed concentration information in the third

P. M. Oates (✉) · C. F. Harvey
Ralph M. Parsons Laboratory,
Department of Civil and Environmental Engineering,
Massachusetts Institute of Technology,
Cambridge, MA 02139, USA
e-mail: pproof@mit.edu

dimension is more valuable depends on what questions the researchers are trying to answer.

To study reactive mixing with light absorption imaging, a reaction is needed where two initially colorless reagents react to form a colored, stable, soluble, quantitative product. Ideally, this reaction should happen at circumneutral pH, not involve hazardous chemicals, and be unreactive with other materials used in the study. Unfortunately, this type of reaction is very hard to find (Breidenthal 1981). Several reactions have been used for flow visualization: ozone and nitric oxide for turbulent jet studies (Shea 1977); photochemically induced colorimetric reactions for hydrodynamic instabilities at reactive interfaces (Avnir and Kagan 1984); iron(II) and nitric acid for studying multicomponent convection (Pojman et al. 1991); electrically induced iodate–arsenous acid reaction to produce iodine in the presence of starch (Bockmann and Muller 2000); phenolphthalein and base, which is probably the most commonly used reaction to study fluid–fluid mixing (e.g. Menisher et al. 2000; Fox and Gex 1956; Zhang et al. 1995; Breidenthal 1981); and recently Gramling et al. (2002) used a complexation reaction of copper sulfate and EDTA.

We found that all of the above-mentioned reactions had undesirable characteristics for studying fluid–fluid mixing. While the phenolphthalein reaction contains many of the desired attributes (Breidenthal 1981), the colored product is unstable and fades back to colorless (Nicholson 1989); thus, it only allows for the calculation of a lower mixing bound (Breidenthal 1981). Gramling et al. (2002) overcame this problem of color stability by using a copper sulfate–EDTA reaction that forms a dark blue complex, but the copper sulfate reagent is initially light blue, making it impossible to distinguish between reagent and low product concentration. While an ideal reaction may not exist, we sought to improve the colorimetric reaction used for absorption imaging. In addition to the above-mentioned reactions, we also considered leuco crystal violet and hydrogen peroxide, manganese and periodate, but they all failed to meet one or more of the aforementioned requirements. We found the colorimetric reaction of Tiron (1,2-dihydroxybenzene-3,5-disulfonic acid) and molybdate suitable to quantifiably study the mixing of two fluids.

In Sect. 1 of this paper, we give the background on Tiron, molybdate, and their complexation reaction. Next, we present a specific chemical recipe and its properties relevant to study fluid–fluid mixing, cover the governing reaction equations, and model the reaction to fit two chemical equilibrium constants. Then we discuss how light absorbance captured by a digital camera relates to product concentration. Finally, we discuss some practical implementation issues and then give an example of imaged absorbance of this reaction used to study mixing in transparent heterogeneous porous media.

2 Tiron, molybdate, and their reaction

1,2-Dihydroxybenzene-3,5-disulfonic acid:

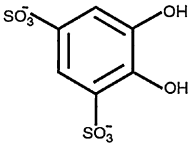

was named Tiron for its use as a chelatometric indicator for both titanium and iron (Yoe and Armstrong 1947). Tiron is easily soluble in water, slightly soluble in alcohol, and insoluble in nonpolar organic solvents. The ionization constants for the two hydroxyl groups are $pKa_1 = 7.66$ and $pKa_2 = 12.6$ (Schwarzenback and Willi 1951). Aqueous solutions are colorless (Atkinson and McBryde 1957; Will and Yoe 1953) and have been reported to remain stable for a year (Atkinson and McBryde 1957). However, Tiron easily oxidizes in alkaline solutions to turn colored (Atkinson and McBride 1957), and we found it to slightly photooxidize after sitting exposed to light after about a week. Tiron forms colored complexes with Fe^{+3}, MoO_4^{-2}, OsO_5^{-2}, Cu^{+2}, UO_2^{+2}, VO^{+2}, Ti^{+4} (Will and Yoe 1953) and many rare earth metals (Taketatsu and Toriumi 1970, 1971); it forms colorless complexes with Al^{+3}, Ca^{+2}, Ce^{+3}, Sn^{+4}, Zr^{+4}, Th^{+4}, Hg^{+2}, WO_4^{-2}, Pb^{+2}; and Tiron reduces Ag^{+} and $AuCl_4^{-}$ to the metallic state (Will and Yoe 1953).

Molybdate oxo species polymerize depending on the concentration and pH of the solution (Aveston et al. 1964; Mitchell 1990). Under conditions of a pH between 0.9 and 6.0 and molybdate concentrations greater than 10^{-3} M, MoO_4^{2-} anions form $[Mo_7O_{24}]^{-6}$ and $[Mo_8O_{26}]^{-4}$ polymeric species. Below a pH of 0.9, molybdate precipitates as MoO_3. Above a pH of 7, it forms ''molybdenum blues'', which is a blue mixture of molybdenum(VI) and molybdenum(V) oxyhydroxides, typically represented as $[Mo_3^{6+}Mo_3^{5+}O_{18}H]^{-}$. However, between a pH of 6 and 7, molybdate exists as monoanions, which are clear in solution (Mitchell 1990). When the molybdate ion hydrates, it can act acidic (the exact degree of protonation is pH dependent; $pKa_1 = 4.24$, $pKa_2 = 8.24$ (Flaschka and Barnard 1967):

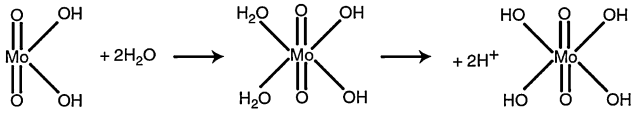

The final product can be described as the tetrahydroxo complex of the molybdenyl(VI) cation, MoO_2^{2+}, which will complex with anionic chelating agents (Flaschka and Barnard 1967).

Dozens of polyphenolic compounds have been reported to react with molybdenum (Flaschka and Barnard 1967) via the chelating agent displacing the molybdate hydroxo ligands (see below) to form a stronger complex (Schwarzenback 1957). The general structure of the polyphenolic-molybdenum chelate is given by Flaschka and Barnard (1967):

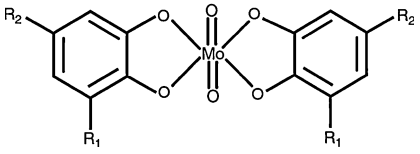

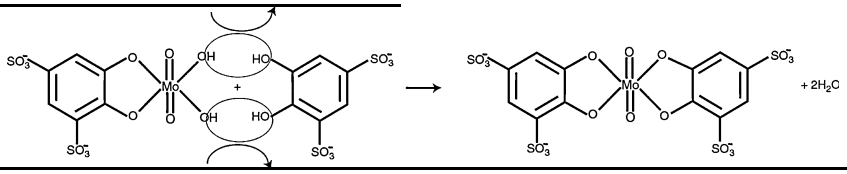

In the case of Tiron, the two R groups (R_2 and R_1) are sulfonate groups ($-SO_3^-$), which are responsible for the high water solubility of Tiron and its complexes. Tiron was found to be the most stable molybdate ligand of EDTA, NTA, or 5-sulfosalicylic acid (Chabarek et al. 1959) and the complexation occurs instantaneously to produce a color that is stable for at least 3 weeks (Will and Yoe 1953). Furthermore, Will and Yoe (1953) recommended this reaction for the spectrophotometric determination of molybdate. Two Tiron–molybdate species with a metal to ligand ratio of 1:1 and 1:2 have been reported (Flaschka and Barnard 1967). The first complexation reaction can be written as:

$$\mathrm{Ti} + \mathrm{Mo} \rightleftharpoons \mathrm{MoTi} \tag{1}$$

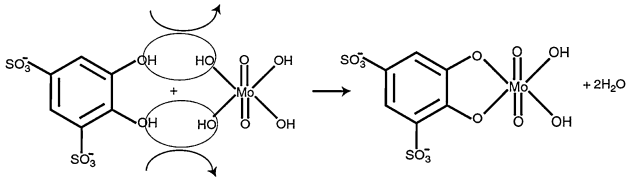

where Ti is the molar concentration of Tiron, Mo is the molar concentration of molybdate, and MoTi is the molar concentration of the 1:1 complex. This dehydration can produce H_3O^+ or OH^- as well as H_2O depending on the pH of the solution (Flaschka and Barnard 1967). In a well-buffered solution, this first reaction can be expressed with the equilibrium expression:

$$K_1 = \frac{[\mathrm{MoTi}]}{[\mathrm{Mo}][\mathrm{Ti}]} \tag{2}$$

where K_1 is the first equilibrium constant (l/mol). This first product then undergoes an additional reaction with Tiron to produce the complex in the form reported by Flaschka and Barnard (1967):

$$\mathrm{MoTi} + \mathrm{Ti} \rightleftharpoons \mathrm{MoTi_2} \tag{3}$$

where $MoTi_2$ is the second chelate formed. The second equilibrium expression follows:

$$K_2 = \frac{[\mathrm{MoTi_2}]}{[\mathrm{MoTi}][\mathrm{Ti}]} \tag{4}$$

where K_2 is the second equilibrium constant (l/mol).

Mixing two clear solutions of 0.05 M Tiron and 0.025 M molybdate buffered at pH 6.1 (see next section for exact recipe) forms a red wine color, which progressively appears orange and then yellow as the products are diluted. The colored products strongly absorb in the violet and blue region of the spectrum, transmit the yellow and red wavelengths, and the absorbance of green light increases with product concentration. The red-to-yellow color shift occurs because green and red light transmitted together appears as yellow (Serway and Faughn 1995). Thus, at low concentrations, the product solution transmits green, yellow, and red; the combination of green and red with the yellow gives the solution a yellow appearance. However, as product concentrations increase, the complexes absorb more of the green wavelengths. Without green light, the transmitted wavelengths progressively appear redder and the solution changes from yellow to orange to red.

3 A chemical recipe to study fluid mixing in thin laboratory chambers

We chose reagent concentrations of 0.05 M Tiron (added as a disodium salt) and 0.025 M molybdate (added as ammonium molybdate) in order for a digital camera to record the colored product absorbances with a dynamic range of over 1.5 orders of magnitude in a clear tank approximately 0.7 cm thick. A pH of 6.1 was chosen so molybdate would predominantly exist in the mono-anionic form allowing the diffusion coefficients of all reacting species to be explicitly calculated and accounted for in a model if desired. Additionally, at pH 6.1, alkaline-induced oxidation of Tiron is minimized, reducing absorbance artifacts. We used a 0.13 M succinate buffer (added as succinic acid) to ensure no spatial or temporal pH changes, which would make the observed color more difficult to understand, as the reaction is pH sensitive. Succinate was chosen because its second p*K*a is 5.64, close to the desired pH, and it had no adverse effects on the reaction. Finally, sodium chloride was added to the molybdate solution to equalize its density to the Tiron solution.

In summary, the species concentrations in the two solutions buffered at a pH of 6.1 were:

- *Tiron solution*: 0.05 M Ti ($pKa_1 = 7.66$, $pKa_2 = 12.6$); 0.356 M Na; 0.13 M succinate ($pKa_1 = 4.21$, $pKa_2 = 5.64$).
- *Molybdate solution*: 0.025 M Mo ($pKa_1 = 4.24$, p*K*a2 = 8.24); .0.215 M NH_4 (p*K*a = 9.25); 0.477 M Na; and 0.192 M Cl, 0.13 M succinate.

We also investigated the viscosity of the two solutions and calculated the diffusion coefficients of all the species involved, as these factors might be important for reactive transport situations. Using a Cannon–Fenske Routine Viscometer in triplicate, we found no distinguishable difference between the kinematic viscosity of the Tiron, molybdate, or product solution (equal volumes of 0.05 M Tiron with 0.025 molybdate). The average viscosity of the three solutions was 0.9798 ± 0.0017 mm^2/s at 25°C (H_2O = 1.1526 mm^2/s), where the uncertainty is in the range of our experimental error. The self-diffusion coefficients not found in the literature were calculated by the method of Hayduk and Laudie (1974), which relates the molecular diffusion in water (cm^2/s) to the species molar volume calculated by the method of Fuller et al. (1966). The self-diffusion coefficients for the species considered are given in Table 1.

4 Tiron and molybdate reaction model

At a pH of 6.1, the predominant species and their charges are Na^+ (over 96% of the cations by concentration are sodium and we considered it the only cation in system); Ti^{-2} (>97% diprotonated); Mo^{-1} (>98% mono-prononated); and 74% $Succ^{2-}$ and 26% $SuccH^-$. These will be the species considered in the model. The colorimetric reactions can be modeled as (the specifics of the reaction will be developed below):

$$\begin{aligned} Mo^{-1} + Ti^{-2} &\rightleftharpoons MoTi^{-3} + 2H_2O \\ MoTi^{-3} + Ti^{-2} &\rightleftharpoons MoTi_2^{-4} + OH^- + H_2O \end{aligned} \tag{5}$$

We assumed that because of succinate's p*K*a's and high concentration, it is the only species to react with the OH^- and that the reaction occurs rapidly.

$$SuccH^{-1} + OH^- \rightleftharpoons Succ^{-2} + H_2O \tag{6}$$

The rapid reaction assumption was supported by the experimental observation that the pH did not change during the reaction. If the colorimetric reaction is rapid and produces OH^- as supported by the literature and experimental observation in an unbuffered solution at pH = 6.1, the quenching of OH^- must also be instantaneous or the pH would change. Therefore, because $MoTi_2^{-4}$ is equal to the amount of OH^- produced, we can assume:

$$\begin{aligned} SuccH^{-1} &= (SuccH^{-1})_0 - MoTi_2^{-4} \\ Succ^{-2} &= (Succ^{-2})_0 + MoTi_2^{-4} \end{aligned} \tag{7}$$

Table 1 Diffusion coefficients

Species	Ti^{-2}	Mo^{-1}	$Succ^{-2}$	$SuccH^{-1}$	Cl^-	$MoTi^{-3}$	$MoTi_2^{-4}$	Na^+
Free solution self-diffusivity[a] (cm^2/s)	5.4×10^{-6}[b]	1.98×10^{-5}[c]	9.6×10^{-6}[b]	9.4×10^{-6}[b]	2.03×10^{-5}[c]	5.1×10^{-6}[b]	3.3×10^{-6}[b]	1.334×10^{-5}[c]

[a] For suggested recipe multiply by 0.98 for viscosity corrections

[b] Calculated from Hayduk and Laudie (1974) and Fuller et al. (1966)

[c] Taken from CRC

where $SuccH_0^{-1}$ and $SuccH_0^{-2}$ are the initial concentration of protonated and unprotonated succinate, respectively.

When the concentrations are mixed, mass balances for the total molybdate, Mo_T, and the total Tiron, Ti_T, can be written as

$$\begin{aligned} Ti_T &= Ti + MoTi + 2MoTi_2 \\ Mo_T &= Mo + MoTi + MoTi_2 \end{aligned} \tag{8}$$

Combining Eq. 8 with Eqs. 2 and 4 redefines the two equilibrium expressions:

$$K_1 = \frac{[MoTi]}{[Mo_T - MoTi - MoTi_2][Ti_T - MoTi - 2MoTi_2]} \tag{9}$$

$$K_2 = \frac{[MoTi_2]}{[MoTi][Ti_T - MoTi - 2MoTi_2]} \tag{10}$$

Equations 9 and 10 can be solved simultaneously to obtain independent analytic solutions for each of the product complexes:

$$\begin{aligned} [MoTi] &= f([Ti_T], [Mo_T], K_1, K_2) \\ [MoTi_2] &= f([Ti_T], [Mo_T], K_1, K_2) \end{aligned} \tag{11}$$

The solutions found using Matlab are too lengthy for presentation in this paper. Because Beer's Law is additive, the linear absorbance, A_1, of the two products can be expressed as:

$$-\log\left(\frac{T}{T_0}\right) = A_1 = \varepsilon_1[MoTi] + \varepsilon_2[MoTi_2] \tag{12}$$

where T/T_0 is the fraction of light transmitted; and ε_1 and ε_2 are coefficients that include the transmittance path length (1 cm in our experimental tank) and the corresponding molar absorptivity of the compound. It is expected that the complexed species with two Tirons absorb more light because it has more delocalized electrons (larger antenna to absorb light).

5 Equilibrium constants

The two stock reagent solutions described above were combined in incrementally increasing ratios of Mo to Ti to make 30 samples with identical total volumes (actual concentrations of Mo_T and Ti_T can be read from Fig. 1). The resulting absorbances were measured with a Beckman DU 640 spectrophotometer at 580 nm with a 1 cm cuvette. Replicate absorbances were created with a different brand of chemical reagents

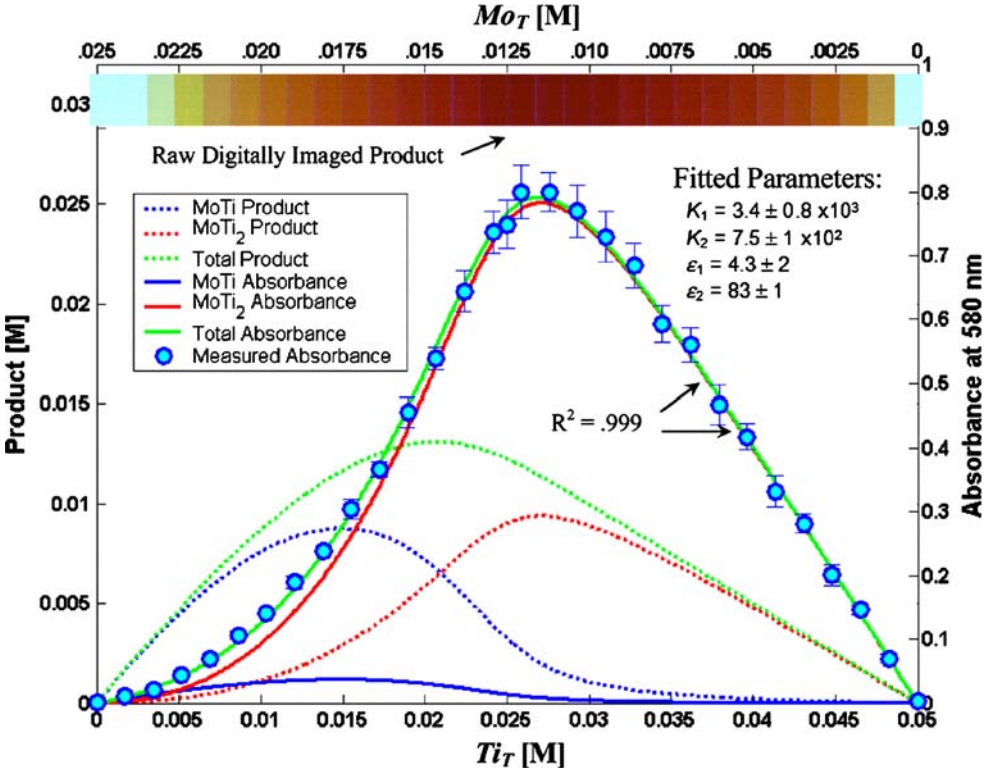

Fig. 1 Modeling the Tiron–molybdate reaction to fit K_1 and K_2 at pH = 6.1. This figure is read by looking at the top and bottom x-axis of respective total Tiron and total molybdate concentrations that formed the product concentrations (left y-axis) and corresponding absorbances at 580 nm (right y-axis)

(originally Sigma and then Fluka) on a different day to produce absorbances within 5% of each other.

Utilizing Eqs. 11 and 12, a Gauss–Newton nonlinear least squares minimization was used to fit K_1, K_2, ε_1, and ε_2 to the observed absorbance at 580 nm. Different initial guesses were used for the same estimation to confirm that the parameters converged to a unique value. Conventional methods were used to calculate the standard deviations on each of the fitted parameters from the Jacobian matrix (derivatives of residuals with parameter values) at the solution and the residuals (Milton and Arnold 1995). The model gave an excellent fit to the data (Fig. 1) to produce the following parameter values: $K_1 = 3.4$ (0.8×10^3 l/mol, $K_2 = 7.5$ (1×10^2 l/mol, $\varepsilon_1 = 4.3 \pm 2$ l/(mol cm), $\varepsilon_2 = 83 \pm 1$ l/(mol cm).

These fitted K values should be applicable to a wide range of combinations of molybdate and Tiron concentrations over a wide range of wavelengths as long as the pH is maintained at 6.1. A parameter sensitivity analysis was conducted by determining the change to sum of the squared residuals caused by decreasing each of the following parameters by 5%: Mo_T, Ti_T, K_1, K_2, ε_1, and ε_2. The parameter rank from most sensitive to least sensitive including the resulting % change of the sum of squared residuals is ε_2 (520%), Ti_T (410%), Mo_T (360%), K_2 (11%), K_1 (2.2%), ε_1 (1%). At a pH of 6.1 and a wavelength of 580 nm, absorbance is dominated by the $MoTi_2$ species. If the model is simplified (incorrectly) by setting the absorbance of MoTi to zero, then the best fit has a 15% higher root mean square error, although the total error is still very low. However, treating $MoTi_2$ as the only absorbing species may serve to be a good first approximation.

6 Imaged absorbance versus monochromatic absorbance

Digital cameras that record polychromatic absorption provide a practical tool for studying spatial patterns of color-changing reactions in experimental tanks. The observed color shift from yellow to orange to red led us to investigate the relationship between the recorded polychromatic absorption and the monochromatic absorbance predicted by Beer's law. The cuvette containing the product solutions (same solutions as in Sect. 5) was placed in front of a sophisticated light box designed to give a constant source of diffuse white light (see Detwiler et al. 1999 for details). An Optronics MagnaFire 10 bit (1024×1024 pixel) digital camera (designed for quantitative scientific imaging) was placed 2 ft in front of the cuvette on the opposite side of the light box to take digital images with an exposure time of ~0.6 s. The resulting images were processed with IP Lab to convert pixel intensities towards the center of the cuvette into normalized absorbances according to Beer–Lambert Law:

$$\frac{A_i}{A_O} = \frac{\log(I_i) - \log(I_{\text{blank}})}{\log(I_{\max}) - \log(I_{\text{blank}})} \tag{13}$$

where A_i is the absorbance of the ith product solution, A_O is the maximum product absorbance, I_i is the measured light intensity of ith product solution, I_{blank} is the measured light intensity of the blank solution, $I_{\max}$ is the measured light intensity of the max product solution. The resulting normalized absorbances varied little over the cuvette and an average value was used. We found the relationship between the recorded polychromatic absorption and the monochromatic absorbance is nonlinear, but very well described by an exponential function (Fig. 2).

This result is explained by considering absorbance curves over the full visible spectrum on the spectrophotometer. Fifteen samples were prepared as previously described, and the concentrations of MoTi and $MoTi_2$ were calculated using the best-fit equilibrium constants. Then the absorbance over the visual spectrum, which is what the digital camera observes, was compared to the absorbance at 580 nm (Fig. 3).

Beer's law is valid for monochromatic light and states that absorbance is linear with concentration. However, nonlinear behavior is often observed at high absorbance values because of measurement limitations and an increase in the refractive index as the solution becomes more concentrated. For the MoTi and $MoTi_2$ species, shorter wavelengths are significantly

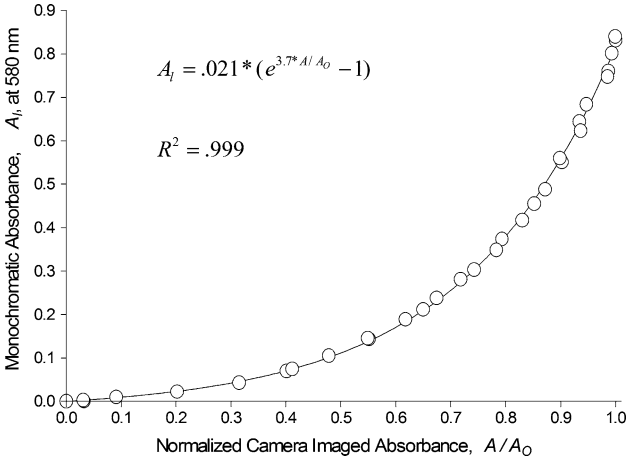

Fig. 2 Monochromatic absorbance versus normalized imaged absorbance

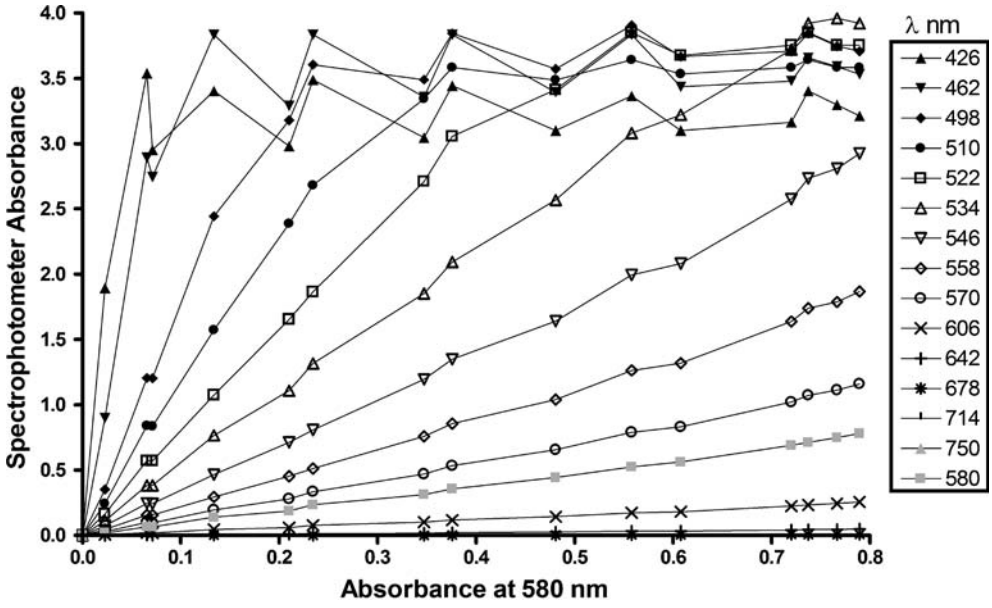

Fig. 3 Comparing absorbance over the visible spectrum as the product concentration increases

transmitted at low product concentrations and they make up a portion of the observed light as seen by the digital camera. However, as the product concentration increases the shorter wavelengths plateau while the higher wavelengths are still absorbed in proportion to the concentration, implying that at high concentrations the short wavelengths are below the detection limit, which also verifies the progressively redder appearance of the product solution (see Sect. 2). Therefore, the plateauing absorbance of lower, but not higher, wavelengths with increasing product concentration explains the nonlinear behavior of digitally imaged camera absorbances and concentrations. The wave-like appearance of the higher absorbance values is systematic with the crests having predominantly MoTi and the troughs having predominantly $MoTi_2$. This implies the ratio of MoTi to $MoTi_2$ molar absorbtivities (ε_1 and ε_2) at the lower wavelengths (and higher absorbances) is higher than the implemented value determined at 580 nm. The only importance of this is MoTi does seem to have a more significant absorbance in the visible spectrum than determined from the fit at 580 nm. Because Beer's law is valid for monochromatic light, we can transform camera absorbances, A/A_O, into linear absorbances, A_l, through the following relationship (see Fig. 2):

$$A_l = \kappa_1(e^{\kappa_2 A/A_O} - 1) \tag{14}$$

where κ_1 and κ_2 are fitted coefficients. Pixel-by-pixel calibration curves to fit κ_1 and κ_2 (Eq. 13) can be constructed from linear absorbances measured by a spectrophotometer, such as at 580 nm, and digitally imaged absorbances of the physical system containing the same product concentrations. These pixel-by-pixel calibration curves allow for absorbances captured by the digital camera to be converted into linear absorbances, which can then be compared with modeled linear absorbances calculated from modeled product concentrations.

7 Practical implementation: an example of imaged absorbances of mixing and reaction in heterogeneous porous media

We have presented a colorimetric reaction and relevant properties to fluid mixing that starts with two colorless reagents which upon mixing instantly form colored, stable, soluble, quantitative products that can be modeled and used to assess fluid mixing. However, before implementing this reaction, there are some practical issues worth addressing. At a concentration of 0.05 M and pH of 6.1, Tiron has a very slight absorbance, which may be non-negligible if the path length is above a few centimeters. Additionally, if a fluid–fluid system is being studied at slow flow rates and is constantly exposed to light, Tiron may photo-oxidize and turn slightly colored. There are several alternatives to overcome these Tiron absorbance artifacts. First, if the path length of the system is longer than 1 cm, the Tiron and molybdate concentrations can be decreased because the absorbance of both the colored product and Tiron varies linearly with path length. The decrease in product concentration will directly offset the increase in path length and would still be visible to the digital camera over 1.5 orders of magnitude.

Additionally, if explicitly modeling the diffusion of each species is unimportant (and there are no concerns with molybdate polymerizing), the pH of the solution could be lowered to minimize Tiron absorption as long as new K_1 and K_2 are determined. For experiments run for several days, photo-oxidation can be minimized by shutting off the light source or blocking it with an opaque barrier between snapshots. Additionally, Tiron solutions should be stored in the dark to minimize photo-oxidation. Lastly, because Tiron complexes with many metals (see Sect. 1), metals must be absent from the fluid–fluid system. For example, we found that trace amounts of iron in our system react with Tiron to form a deep purple color. Iron was subsequently removed by magnetic separation. With these issues resolved, this reaction can be very useful for studying fluid–fluid mixing.

For example, we used the Tiron–molybdate reaction to image fluid–fluid mixing in heterogeneous porous media. Assuming solutes are not sorbing to the porous media, mixing in porous media is a result of hydrodynamic dispersion (pore-scale and local velocity variations), which leads to the spreading and stretching of solute plume interfaces. This stretching itself does not mix solutes, but it greatly enhances the surface areas for solutes to diffuse. Concentrations of reactants C are typically calculated by modeling transport with a hydrodynamic dispersion coefficient D from the advection–dispersion equation:

$$\frac{\partial C}{\partial t} = D\frac{\partial^2 C}{\partial x^2} - v\frac{\partial C}{\partial x} \tag{15}$$

where v is the average linear velocity. This model implicitly averages reacting concentrations at the pore scale and larger length scales in heterogeneous formations; this incorrectly assumes complete mixing and leads to an over prediction of mixing and reaction (e.g. Kapoor et al. 1997; Ginn et al. 1995; Miralles-Wilhelm et al. 1997; Gramling et al. 2002; Jose et al. 2004). To help resolve these issues and create up-scaled models of reactive transport in heterogeneous porous media, we used the experimental setup described by Gramling et al. (2002) and the tanks of heterogeneous porous media created by Zinn et al. (2004) with the Tiron–molybdate reaction (Fig. 4).

In this setup, a clear heterogeneous tank ($40 \times 20 \times 0.65$ cm^3) had spatially varying hydraulic conductivity from large glass beads (2.1 mm) packed in 2.5 cm diameter circular inclusions that contained smaller glass beads (0.9 mm) resulting in a hydraulic conductivity ratio of 6, with slower velocities moving through the small circles. The tank was initially

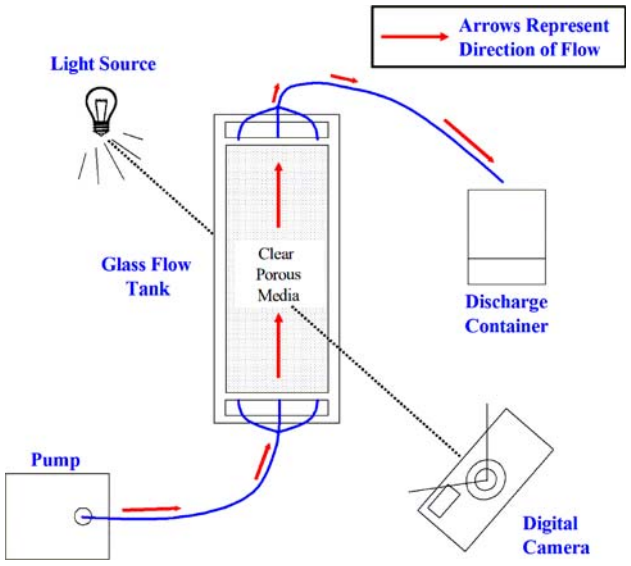

Fig. 4 Experimental setup

saturated with the Tiron solution and a molybdate solution (see Sect. 3 for solution concentrations) was injected with an ISCO model 500D syringe pump at a flow rate of 4.1 ml/min. The chamber was mounted in front of a sophisticated light box designed to give a constant source of diffuse white light (see Detwiler et al. 1999 for details). A 14-bit liquid-cooled CCD camera was placed on the opposite side of the tank at a distance of ~10 ft, which gave a spatial resolution of ~0.3 mm while still capturing the entire 20×40 cm^2 absorbance field, which ultimately produced ~750,000 absorbance values per time snap shot. Images were taken every minute with an exposure time of ~0.7 s. IP Lab was used to process the images to convert pixel intensities into normalized absorbance according to Eq. 13 (Fig. 5).

The normalized camera imaged absorbances were transformed to a linear absorbance by constructing pixel-by-pixel calibration curves from six known Tiron/molybdate mixtures (Table 2) to fit the exponential transform coefficients κ_1 and κ_2 ($R^2 = 0.99 \pm 0.02$) from Eq. 14 at every pixel. A mass balance was then performed by comparing the digitally imaged mass to the known injected mass and the total masses differed by less than 3%, indicating there is fairly low experimental error. The transform coefficients allowed for the observed linear absorbance based on molecular scale collisions to be compared to a model-predicted linear absorbance. The modeled linear absorbance was based on a finite difference of the conventional 1D advection–dispersion equation (Eq. 15) to model the mixing and reaction of Mo_T and Ti_T (Eqs. 11 and 12). The experimental product is inherently averaged over

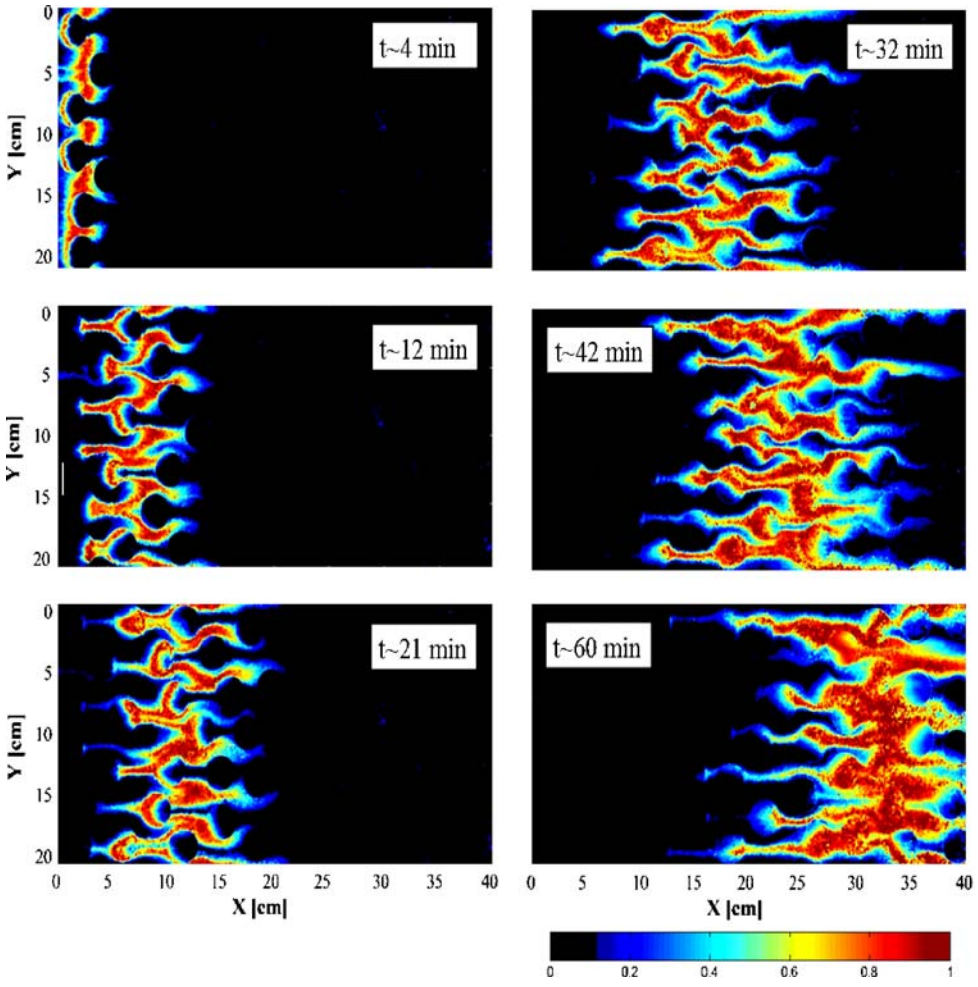

Fig. 5 Imaged absorbances of six time snap shots of fluid–fluid mixing in heterogeneous porous media, elucidated by the Tiron–molybdate reaction. Flow is from left to right

the thickness of the tank but it does provide the correct spatial average of the molecular scale product. Next the product is spatially averaged over Y so that it can be compared to the 1D model along X. Using a Gauss–Newton nonlinear least squares minimization, the best fit dispersion coefficient 0.63 cm^2/min and average linear velocity of 0.57 cm/min does a poor job of modeling the correct amount of mixing and reaction (Fig. 6).

As can be observed from the variability in the Y-direction in Fig. 5, mixing is not complete as assumed by the advection–dispersion equation. This incomplete mixing causes the discrepancy between the observed and model predicted reaction. Up-scaled models to describe reactive transport, as visualized in Fig. 5, do not yet exist and are the focus of our, and many other researchers' studies (e.g. Kitanidis 1994; Kapoor and Kitanidis 1996, 1998; Weeks and Sposito 1998; Oya and Valocchi 1998; Cirpka et al. 1999). We feel that the reaction and analysis method presented in this paper will be instrumental in understanding mixing in porous

Table 2 Calibration curve solutions

Solution no.	1	2	3	4	5	6
Tiron (M)	0.05	0.0053	0.043	0.017	0.033	0.025
Molybdate (M)	0.0	0.022	0.0033	0.016	0.0083	0.0125
A_1 at 580 nm	0.0	0.047	0.26	0.40	0.64	0.83

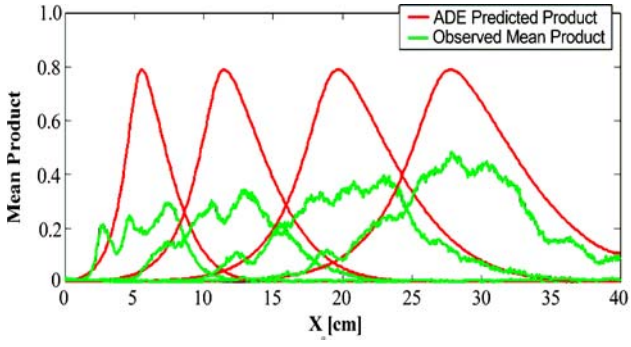

Fig. 6 Comparison of coupling the advection–dispersion equation (ADE) modeled product to the observed product at 8, 18, 32, and 46 min

media and provide the necessary data to develop reactive transport models. Ultimately, it is hoped that this reaction and analysis method will broadly help researchers in industry and academia improve their conceptual and mathematical models of fluid–fluid mixing.

Acknowledgments We would like to thank Claudius Freiherr Von Schwerin and Lucy Meigs from Sandia National Labortories Visual Flow Lab, and Phil Gschwend for his helpful conversation. Funding: NSF and EPA STAR graduate research fellowship. The experiments performed in this paper comply with the current laws of the United States of America.

References

Atkinson GF, McBryde WAE (1957) Oxidation of the analytical reagent ''Tiron'' (disodium-4,5-dihydroxybenzene-1,3-disulphate). Can J Chem 35:477

Aveston J, Anacker EW, Johnson JS (1964) Hydrolysis of molybdenum(VI). Ultracentrifugation, acidity measurements, and Raman spectra of polymolybdates. Inorg Chem 3:735–746

Avnir D, Kagan M (1984) Spatial structures generated by chemical reactions at interfaces. Nature 307:717

Beven KJ, Chatwin PC, Millbank JH, Allen CM (1994) Mixing and transport in the environment: a memorial volume for Catherine M. Allen (1954–1991). Wiley, New York

Bockman M, Muller C (2000) Growth rates of the bouyancy-driven instability of an autocatalytic reaction front in a narrow cell. Phys Rev Lett 85(12):2506–2509

Breidenthal R (1981) Structure in turbulent mixing layers and wakes using a chemical reaction. J Fluid Mech 109:1–24

Chabarek S Jr, Gustafson RL, Courntney RC, Martell AE (1959) Hydrolytic tendencies of metal chelate compounds. III. Oxometal ions. J Am Chem Soc 81:515

Cirpka OA, Frind EO, Helmig R (1999) Numerical simulation of biodegradation controlled by transverse mixing. J Contam Hydrol 40(2):159–182

Detwiler RL, Pringle SE, Glass RJ (1999) Measurement of fracture aperture fields using transmitted light: an evaluation of measurement errors and their influence on simulations of flow and transport through a single fracture. Water Resour Res 35(9):2605–2617

Flaschka HA, Barnard (1967) Chelates in analytical chemistry. Dekker, New York

Fox EA, Gex VE (1956) Single-phase blending of liquids. AICHE J 2(4):539–544

Fuller EN, Schettler PD, Giddings JC (1966) A new method for prediction of binary gas-phase diffusion coefficients. Ind Eng Chem 58:19–27

Ginn TR, Simmons CS, Wood BD (1995) Stochastic-convective transport with nonlinear reaction: biodegradation with microbial growth. Water Resour Res 31(11):2689–2700

Gramling CM, Harvey CF, Meigs LC (2002) Reactive transport in porous media: a comparison of model prediction and laboratory visualization. Environ Sci Technol 36(11):2508–2514

Harnby N, Edwards MF, Nienow AW (1985) Mixing in the process industries (Butterworths series in chemical engineering). Butterworths, Boston

Hayduk W, Laudie (1974) Prediction of diffusion coefficients for non-electrolytes in dilute aqueous solutions. AICHE J 20:611–615

Hickey AJ, Ganderton D (2001) Pharmaceutical process engineering. In: Drugs and the pharmaceutical sciences, vol 112. Dekker, New York

International Union of Biochemistry (1964) International colloquium on rapid mixing and sampling techniques applicable to the study of biochemical reactions: rapid mixing and sampling techniques in biochemistry; proceedings. In: Johnson Research Foundation colloquia. Academic, New York

Jose SC, Rahman MA, Cirpka OA (2004) Large-scale sandbox experiment on longitudinal effective dispersion in heterogeneous porous media. Water Resour Res 40(12):W12415, DOI 10.1029/2004WR003363

Kapoor V, Kitanidis PK (1996) Concentration fluctuations and dilution in two-dimensionally periodic heterogeneous porous media. Transp Porous Media 22:91–119

Kapoor V, Kitanidis PK (1998) Concentration fluctuations and dilution in aquifers. Water Resour Res 34(5):1181–1193

Kapoor V, Gelhar LW, Miralles-Wilhelm F (1997) Bimolecular second order reactions in spatially varying flows: segregation induced scale-dependent transformation rates. Water Resour Res 33(4):527–536

Kitanidis PK (1994) The concept of the dilution index. Water Resour Res 30(7):2011–2026

Kling K, Mewes D (2003) Quantitative measurements of micro- and macromixing in a stirred vessel using planar laser-induced fluorescence. J Vis 6(2):165–173

Koochesfahani M, Dimotakis P (1985) A 'flip' experiment in a chemically reacting turbulent mixing layer. J Fluid Mech 170:83–112

Menisher T, Metghalchi M, Gutoff EB (2000) Mixing studies in bioreactors. Bioprocess Eng 22:115–120

Milton JS, Arnold JC (1995) Introduction to probability and statistics. Principles and applications for engineering and the computing sciences. Irwin/McGraw-Hill, USA

Miralles-Wilhelm F, Gelhar LW, Kapoor V (1997) Stochastic analysis of oxygen-limited biodegradation in three-dimensionally heterogeneous aquifers. Water Resour Res 33(6):1251–1263

Mitchell PCH (1990) Molybdenum and molybdenum compounds. In: Ullmann's encyclopedia of industrial chemistry, 5th edn. A16, 668. Wiley-VCH GmbH & Co. KGaA, Weinheim

Nicholson L (1989) Kinetics of the fading of phenolphthalein in alkaline solution. J Chem Educ 66:725–726

Omurtag A, Stickel V, Chevray R (1996) Chaotic advection in a bioengineering system. In: Proceedings of the eleventh ASCE engineering conference, Fort Lauderdale, FL

Ottino JM (1990) Mixing, *chaotic advection*, and turbulence. Annu Rev Fluid Mech 22:207–253

Oya S, Valocchi AJ (1998) Transport and biodegradation of solutes in stratified aquifers under enhanced in situ bioremediation conditions. Water Resour Res 34(12):3323–3334

Pojman JA, Nagy IP, Epstein IR (1991) Convective effects on chemical waves. 3. Multicomponent convection in the iron(II)–nitric acid system. J Phys Chem 95:1306–1311

Schwarzenback G (1957) Die komplexometrische Titration, Ferd. Enke Verlag, Stuttgart, p 2

Schwarzenbach G, Willi A (1951) Metallindikatoren III. Die Komplexbildung der Brenzcatechin-3,5-disulfosäure (Tiron) mit dem Eisen(III)-ion. Helv Chim Acta 34:528

Serway RA, Faughn JS (1995) College physics. Saunders College Publishing, New York

Shea JR (1977) A chemical reaction in a turbulent jet. J Fluid Mech 81:317–333

Sterbacek Z, Tausk P (1965) Mixing in the chemical industry. 1st edn. International series of monographs in chemical engineering, vol 5. Pergamon Press, Oxford

Taketatsu T, Toriumi N (1970) Spectrophotometric study and analytical application of rare earth tiron complexes-I. Talanta 17:465–473

Taketatsu T, Toriumi N (1971) Spectrophotometric study and analytical application of rare earth tiron complexes-II. Talanta 18:647–649

Tidwell VC, Glass RJ (1994) X ray and visible light transmission for laboratory measurement of two-dimensional saturation fields in thin-slab systems. Water Resour Res 30(11):2873–2882

Weeks SW, Sposito G (1998) Mixing and stretching efficiency in steady and unsteady groundwater flows. Water Resour Res 34(12):3315–3322

Will F, Yoe JH (1953) Anal Chim Acta 8:546

Yoe JH, Armstrong AR (1947) Colorimetric determination of titanium with disodium-1,2-dihydroxybenzene-3,5-disulfonate. Ind Eng Chem Anal. Ed 19:100

Zhang S, Schneider SP, Collicott SH (1995) Quantitative molecular-mixing measurements using digital processing of absorption images. Exp Fluids 19(5):319–327

Zinn B, Harvey CF, Meigs L, Haggerty R, Peplinski W, Freiherr von Schwerin C (2004) Experimental visualization of solute transport and mass transfer processes in spatially heterogeneous porous media. Environ Sci Technol 38(14):3916–3926